Protein Science (1996), 5:565-577. Cambridge University Press. Printed in the USA.

Solution structure and lipid binding of a nonspecific lipid transfer protein extracted from maize seeds

JÉRÔME GOMAR,[1] MARIE-CHRISTINE PETIT,[1,5] PATRICK SODANO,[1] DENISE SY,[1,2] DIDIER MARION,[3] JEAN-CLAUDE KADER,[4] FRANÇOISE VOVELLE,[1,2] AND MARIUS PTAK[1,2]

[1] Centre de Biophysique Moléculaire (UPR CNRS 4301), rue Charles Sadron, 45071 Orléans Cedex 02, France
[2] Université d'Orléans, rue Charles Sadron, 45071 Orléans Cedex 02, France
[3] Laboratoire de Biochimie et Technologie des Proteines, INRA, rue de la Géraudière, BP 1627, 44316 Nantes Cedex 05, France
[4] Laboratoire de Physiologie Cellulaire et Moléculaire des Plantes, URA CNRS 1180, Université Pierre et Marie Curie, 4 place Jussieu, 75252 Paris Cedex 05, France

(RECEIVED August 28, 2995; ACCEPTED January 2, 1996)

Abstract

The three-dimensional solution structure of a nonspecific lipid transfer protein extracted from maize seeds determined by ^{1}H NMR spectroscopy is described. This cationic protein consists of 93 amino acid residues. Its structure was determined from 1,091 NOE-derived distance restraints, including 929 interresidue connectivities and 197 dihedral restraints (ϕ,ψ, χ_1) derived from NOEs and ^{3}J coupling constants. The global fold involving four helical fragments connected by three loops and a C-terminal tail without regular secondary structures is stabilized by four disulfide bridges. The most striking feature of this structure is the existence of an internal hydrophobic cavity running through the whole molecule. The global fold of this protein, very similar to that of a previously described lipid transfer protein extracted from wheat seeds (Gincel E et al., 1994, *Eur J Biochem 226*:413-422) constitutes a new architecture for α-class proteins. ^{1}H NMR and fluorescence studies show that this protein forms well-defined complexes in aqueous solution with lysophosphatidylcholine. Dissociation constants, K_d, of $1.9 \pm 0.6 \times 10^{-6}$ M and $>10^{-3}$ M were obtained with lyso-C_{16} and -C_{12}, respectively. A structure model for a lipid-protein complex is proposed in which the aliphatic chain of the phospholipid is inserted in the internal cavity and the polar head interacts with the charged side chains located at one end of this cavity. Our model for the lipid-protein complex is qualitatively very similar to the recently published crystal structure (Shin DH et al., 1995, *Structure 3*:189-199).

Keywords: lipid binding; lipid transfer protein; maize; molecular modeling; NMR

Lipid transfer proteins, found in various organisms including animals, plants, yeast, and prokaryotic cells (Crain & Zilversmitt, 1980), have the common property of transferring phospholipids between membranes in vitro. Whereas several LTPs extracted from mammalian tissues are specific (Rueckert & Schmidt, 1990), plant LTPs exhibit a broad range of affinity for polar lipids because they transfer (Miquel et al., 1987; Geldwerth et al., 1991) phosphatidylcholine, phosphatidylethanolamine, phosphatidylinositol, and glycolipids; hence their name, nonspecific lipid transfer proteins. These proteins, also able to bind fatty acids and acyl-coenzyme A esters (Ostergaard et al., 1993), constitute a family of small (about 9 kDa) basic proteins, and a consensus sequence (Desormeaux et al., 1992) of more than 15 primary structures of ns-LTPs has been established. The eight cysteines of the sequence are strictly conserved and form a common array of disulfide bridges. Genes and/or cDNAs encoding ns-LTPs have been isolated from a large number of plant species and there are generally several LTP genes per plant genome, except for the carrot, in which only one gene has been detected (Sterk et al., 1991). Two or three ns-LTP genes are present in the *Arabidopsis* genome (Thoma et al., 1994), at least four in the genome of *Brassica olecea* (Pyee et al., 1994), and two in the tomato genome (Torres-Schuman et al., 1992). Several ns-

Reprint requests to: Françoise Vovelle, Centre de Biophysique Moléculaire (UPR CNRS 4301), rue Charles Sadron, 45071 Orléans Cedex 02, France; e-mail: vovelle@cnrs-orleans.fr.

[5] Present address: City College, Department of Chemistry, New York, New York 10031.

Abbreviations: CMC, critical micellar concentration; DQF-COSY, double quantum filtered J-correlated spectroscopy; ECOSY, exclusive J-correlated spectroscopy; HPS, hydrophobic protein from soybean; LTP, lipid transfer protein; lyso-C_{16}, lyso-α-palmitoyl-phosphatidylcholine; lyso-C_{12}, lyso-α-lauroyl-phosphatidylcholine; NOESY, NOE spectroscopy; ns-LTP, nonspecific LTP; ppm, parts per million; RMSD, RMS deviation; Tris, 2-amino-2-hydroxymethylpropane-1,3-diol.

LTP genes are found in the genomes of barley (Gausing, 1994), castor bean (Tsuboi et al., 1992), rice (Vignols et al., 1994), and sorghum (Pelese-Siebenbourg et al., 1994). It should be noted that, within one plant species, LTP genes encode for isoforms with distinct patterns of expression. There is a great diversity of LTP genes. They are located in various tissues, with some of them being expressed specifically in a cell layer (epidermis, for example, for maize genes [Sossountzov et al., 1991]), in an aleurone layer for barley genes (Skriver et al., 1992), in anthers for some LTP genes from rape seeds (Foster et al., 1992) and tomatoes (Aguirre & Smith, 1993), in cotyledons for castor beans (Weig & Komor, 1992), and in the tobacco shoot apex (Fleming et al., 1992). Other genes are induced under specific physiological conditions such as the stems of salt-stressed tomato plants (Torres-Schuman et al., 1992).

In addition, plant ns-LTPs are all synthesized with a leader peptide. For spinach and barley ns-LTPs (Bernhard et al., 1991), it has been shown that the protein is inserted into the lumen of the endoplasmic reticulum in vitro, thus allowing them to enter the secretory pathway. Indeed, they can be secreted into the medium of carrot embryonic cultures (Sterk et al., 1991) and somatic embryos of grapevine (Coutos-Thevenot et al., 1993). They have also been located in the cell wall of epidermal cells of *Arabidopsis* (Thoma et al., 1994), as well as in glyoxysomes of castor bean cotyledons (Tsuboi et al., 1992).

Despite the extensive effort invested in their study, the role of ns-LTPs remains to be elucidated in vivo. Different theories have been suggested as, for example, the formation of cutin by transporting the hydrophobic cutin monomers (Sterk et al., 1991; Meijer et al., 1993). Owing to their antifungal activity in vitro (Molina et al., 1993) they can also be involved in the defense against pathogens, probably due to a membranotoxic effect as observed for thionins (Bowles, 1990).

Recently, we have determined the three-dimensional structure of a wheat ns-LTP (Gincel et al., 1994) on the basis of two-dimensional ^{1}H-NMR data. This structure involves four helices packed against a C-terminal region that adopts a structure composed of a series of turns (Kinemage 1). The most striking feature of this structure is the existence of an internal hydrophobic cavity running through the whole molecule that appears as a potential site for lipid binding (Kinemages 2 and 3).

In order to better understand the biological function of plant ns-LTPs, we have determined the solution structure of the maize ns-LTP, a basic protein extracted from maize seeds. Its activity, probably closely related to its affinity for amphiphilic lipids, is likely to lead to various biotechnological applications (Record et al., 1993). The maize ns-LTP displays about 60% sequence similarities to the wheat ns-LTP and higher transfer activity. In addition, based on an NMR study of maize ns-LTP complexes with lysolecithin, we propose a structure model in which the aliphatic chain of the phospholipid is inserted into the internal cavity of the protein. While our work was in its final stage, the crystal structure of the maize ns-LTP and its complex with a palmitate were published by Shin et al. (1995). Because the coordinates of these structures are not yet available, only qualitative comparisons can be made. The global folds are very similar in solution and in crystal. These structures represent new models of lipid carriers defined as all α-proteins in which an extended hydrophobic molecule can be inserted. The elucidation of the behavior of ns-LTPs in vitro should help clarify the current hypothesis on their biological function.

Results

Structural statistics and global fold

Two-hundred DIANA structures were generated on the basis of 1,091 NOE-derived distance restraints and 197 dihedral restraints. Twenty-six DIANA structures exhibiting a target function ranging from 0.6 to 2 Å^2 were subjected to simulated annealing and energy minimization with XPLOR. Fifteen structures presenting at least 76% of their (ϕ,ψ) dihedral angles in the core region of the Ramachandran maps and a similar secondary structure pattern were selected for further analysis. All these structures are consistent with NMR-derived restraints (Table 1). The average deviations from the experimental constraints are 0.023 Å and 1.1° for distance and dihedral angle, respectively. In addition, these structures show very small deviations from the ideal geometry and have reasonable nonbonded energy

Table 1. *Structural statistics and residual restraint violations of the 15 structures used to represent the solution structure of maize ns-LTP*

RMSD from experimental restraints			
Distance restraints (Å)	0.023 (0.018; 0.028)		
Angle restraints (°)	1.1 (0.79; 1.49)		
Mean number of violations of experimental restraints			
Distance restraints			
Number > 0.2 Å	3.87 (2; 6)		
Angle restraints			
Number > 5°	2.47 (1; 4)		
XPLOR energies[a]			
E_{NOE} (kcal mol^{-1})	14.77 ± 3.31		
E_{cdh} (kcal mol^{-1})	0.06 ± 0.03		
E_{elec} (kcal mol^{-1})	−268.28 ± 9.20		
E_{L-J} (kcal mol^{-1})	−353.32 ± 9.11		
RMSD from idealized geometry			
Bonds (Å)	0.0089 (0.008; 0.009)		
Angles (°)	2.276 (2.232; 2.320)		
Improper angles (°)	1.028 (0.858; 1.193)		
ϕ/ψ Angle distribution			
Percentage of ϕ and ψ angles lying in the CORE region of the Ramachandran plot[b]	76% (72%, 80%)		
RMSDs with respect to the mean structure[c] (Å)			
	Backbone[d]		All non-hydrogen
Residues 2–92	0.82 ± 0.09 (0.71; 1.02)		1.17 ± 0.10 (1.02; 1.40)
Helices[e]	0.57 ± 0.09 (0.46; 0.73)		0.97 ± 0.11 (0.78; 1.18)
C-terminus[f]	1.02 ± 0.20 (0.73; 1.47)		1.38 ± 0.20 (1.04; 1.78)
Pairwise RMSDs (Å)			
	Backbone[d]		All non-hydrogen
Residues 2–92	1.10 ± 0.16 (0.72; 1.55)		1.70 ± 0.18 (1.30; 2.15)
Helices[e]	0.83 ± 0.16 (0.52; 1.26)		1.41 ± 0.18 (0.95; 1.90)
C-terminus[f]	1.50 ± 0.32 (0.76; 2.26)		2.00 ± 0.36 (1.15; 2.79)

[a] These energy terms are calculated from the final coordinates using the CHARMM force field implemented in XPLOR.

[b] Calculated using Procheck (Laskowski et al., 1993).

[c] The mean structure was obtained by fitting N, Cα, C′, and O for residues 1–93.

[d] The backbone is defined as comprising the N, Cα, C′, and O atoms.

[e] Helices: residues 5–19, 26–39, 43–58, 65–75.

[f] C-terminus: residues 76–92.

terms as underlined by the average electrostatic and van der Waals energy terms (Table 1).

The NMR solution structure of the maize LTP is globular, with overall dimensions of approximately 38 Å by 28 Å by 24 Å. A ribbon representation of the solution structure of this protein (Fig. 1 and Kinemage 1) shows that the global fold involves four helices connected by three loops, a C-terminal fragment without canonical hydrogen bonded structure (Kabsch & Sander, 1983), and four disulfide bridges stabilizing its architecture. The helical parts of the structure are especially well defined by the experimental data as underlined by the RMSD on atomic coordinates of the helix atoms (Table 1). In Figure 2 and in Kinemage 1, one can clearly estimate the quality of the structure determination illustrated by the superposition of the Cα traces for the 15 structures. However, the RMSD for the loops connecting the helices and for the C-terminus (1.5 Å on backbone atoms) are more variable and no unique conformation is determined by NMR data. Globally, there is a good correlation between the number of NOE restraints per residue and the RMSD plot (Fig. 3A,B). The variability of the structures is also illustrated by the (ϕ,ψ) angle variation along the sequence (Fig. 3C,D).

The secondary structure pattern determined using the Kabsch and Sander (1983) method includes four α-helices, H1 (5–19), H2 (26–39), H3 (43–58), and H4 (65–75) (Kinemage 2). One hydrogen bond links Asn 67 side chain to the CO of Tyr 17. The four helices form an original right-handed fold already observed for wheat ns-LTP (Gincel et al., 1994) and hydrophobic protein from soybean (Baud et al., 1993). The maize C-terminal fragment (from Cys 76 to Asn 93) is stabilized by two hydrogen bonds: NH (Ser 84)···O_γ (Thr 87) and O_δ (Asp 88)···NH (Arg 91). Although several residues (Ile 79, Tyr 81, Thr 82, Thr 87, and Asp 88) are found in an extended conformation, the NOE connectivity pattern of this fragment does not correspond to a β-structure. A kink is observed in helix H1 at the Pro 13 residue, disrupting the pattern of α-helical hydrogen bonding. This helix can be divided into two parts, H1a and H1b (Fig. 1). The angle between H1a and H1b is approximately 20°, in agreement with the average value found by X-ray structure statistical analysis for the helices including a proline residue (MacArthur & Thornton, 1991). This kink is important for the organization of the hydrophobic core of the protein. The H4 helix is slightly curved, but there is no marked effect of the Pro 72 residue located at the end of the helix and buried in a hydrophobic environment.

Disulfide bonds

The consensus sequence for vegetable ns-LTPs (Desormeaux et al., 1992) includes eight cysteines forming four disulfide bridges. Only two of them were chemically determined for the castor bean ns-LTP (Takishima et al., 1988) (4–52, 50–89, in the maize numbering), sharing 47.8% of the sequence identities with the maize ns-LTP. A complete assignment of the disulfide bridge, in agreement with the castor bean pairing, was proposed previously for our NMR-derived structure of the wheat ns-LTP (Gincel et al., 1994) and fully confirmed here for the maize ns-LTP using two approaches. In the first step, two disulfide bridges (14–29, 50–89) were assigned unequivocally on the ba-

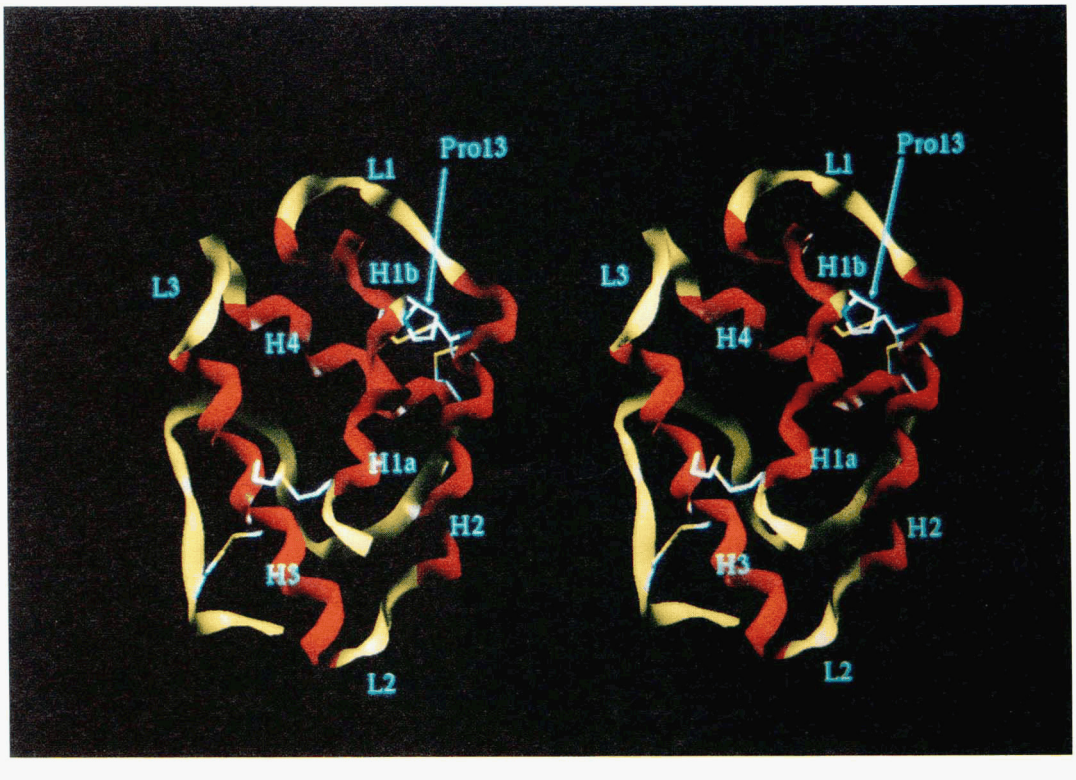

Fig. 1. Stereo view of the main-chain fold of the maize ns-LTP. Side-chain heavy atoms of cysteines in the disulfide bridges and Pro 13 residue are represented in a "capped-stick" style.

Fig. 2. Cα stereo view of best-fit superposition of the 15 final NMR structures of the maize ns-LTP.

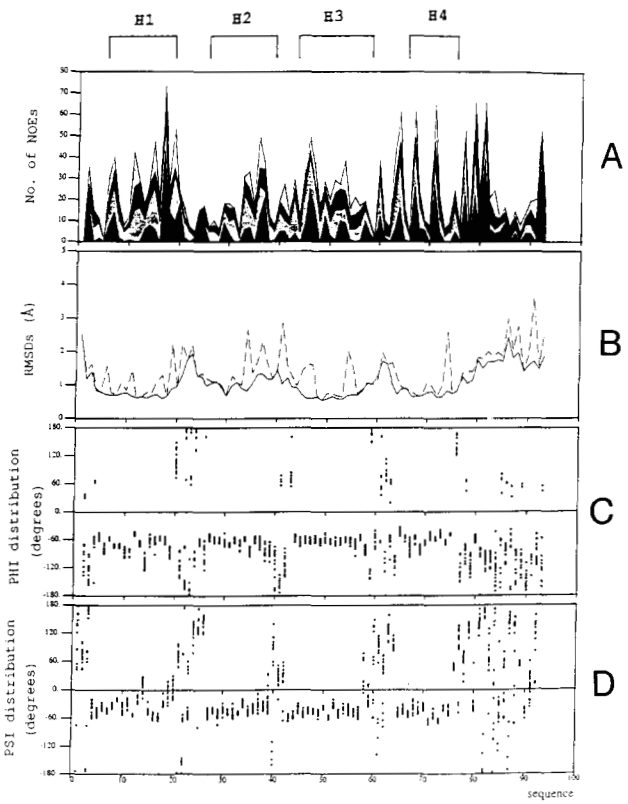

Fig. 3. Structural data for the 15 selected NMR-structures of maize ns-LTP plotted as a function of sequence. Regular secondary structure patterns are indicated in the upper panel. **A:** Distribution of intraresidual (very light shadowed area), sequential (dark area), medium (light shadowed area), and long (dark shadowed area) upper-bounds distances. Restraints are counted for both involved atoms. **B:** Average local RMSD for backbone heavy atoms (N, Cα, C′, and O, solid line) and for all non-hydrogen atoms (dashed lines) obtained by fitting N, Cα, C′, and O for residues 1–93. **C:** Distribution of phi dihedral-angle values. **D:** Distribution of psi dihedral-angle values.

sis of interresidual NOE connectivities, whereas the other two, for which such connectivities were ambiguous, were positioned with the assumption that the disulfide bridge network was identical to that of the wheat ns-LTP (4–52, 30–75). Considering such a network, the consistency of the NOE assignments was tested by performing several rounds of distance geometry structure calculations and NOESY spectra assignments using DIANA (Güntert et al., 1991) and ASNO (Güntert et al., 1993) programs. The (4–52) and (30–75) bridges appeared to be fully compatible with the overall NOE connectivities. In the second step, in order to verify that no other disulfide pairing was compatible with the NOE connectivities, a control calculation was run using DIANA, starting from 50 random structures in which all restraints relative to the disulfide network were removed. The 50 resulting structures were then analyzed in terms of S-S distances. From Table 2, it is clear that the disulfide arrangement is as follows: 4–52, 14–29, 30–75, and 50–89. This disulfide network is the only possible one in agreement with the NOE con-

Table 2. *Average measured S-S distances (Å) in 50 distance geometry structures without disulfide bridge constraints in maize ns-LTP*[a]

S-S	4	14	29	30	50	52	75
14	16.36						
29	15.97	**2.08**					
30	21.16	6.67	5.84				
50	12.51	16.73	16.67	20.09			
52	**3.34**	14.35	14.13	19.33	10.07		
75	19.10	5.05	4.30	**2.78**	17.47	17.07	
89	12.55	19.54	19.41	23.06	**3.82**	10.67	20.48

[a] Values in bold indicate the disulfide pairings with the lowest mean S-S distance.

nectivity pattern. This disulfide pairing agrees with that found previously for the wheat ns-LTP and determined recently by X-ray crystallography for the maize protein (Shin et al., 1995). The four disulfide bridges are located by pairs on the two opposite sides of the molecule (Fig. 1 and Kinemage 2), whereby the H3 helix is linked to the C-terminus and the N-terminal region on one edge, and the H2 helix to the H1 and to the end of the H4 helix on the other.

Hydrophobic core and molecular surface

As with most globular water-soluble proteins, the three-dimensional structure of the maize ns-LTP includes a hydrophobic core constituted by side chains pointing toward the interior of the molecule. As described previously for the wheat ns-LTP, these side chains adopt a special arrangement, forming an elongated cavity running through the whole molecule (Fig. 4 and Kinemage 2). This hydrophobic tunnel-like cavity results from the organization of the four amphipathic helices and from the packing of the C-terminus on the H3 helix from Ser 86 to Ser 89 and on the H4 from Ile 79 to Ile 83. The kink induced by Pro 13 in the H1 helix narrows this hydrophobic cavity (Fig. 4), which can be included in a 20-Å-high cylinder with an elliptic base (3 * 4 Å). Its inner surface involves Val 7, Ala 10, Ile 11, Ile 15, Ala 18 in the H1 helix; Val 33, Leu 36, Ala 40 in the H2; Ala 49, Leu 53, Ala 56, Ala 57, Val 60 in the H3; Leu 63 in L3, Ala 68, Ile 71, Pro 72 in the H4; and Val 77, Ile 79, Ile 83 in the C-terminal region. The presence of such a cavity should allow the insertion of a hydrophobic substrate without major changes in the protein conformation (see below). Both extremities of the hydrophobic cavity are surrounded by solvent-exposed residues Asn 37, Asn 38, Arg 41, Asp 45, Arg 46, and Arg 47 on one side, Arg 19, Gln 21, Asn 64, and Asn 67 on the other. Tyr 81, which probably plays an important role in lipid complexation (see below), lies across the hydrophobic cavity.

The maize ns-LTP is a highly charged protein at neutral pH. At the acidic pH (5.4) used in NMR experiments, the electrical charge of the protein should remain nearly the same (the sequence does not include histidine residues). Figure 5A shows the distribution of charged residues in one of the NMR solution structures of the maize ns-LTP and Figure 5B the electrostatic potential map on the surface of the protein calculated using the MOLCAD (Heiden et al., 1993) option of SYBYL software. Most positively charged side chains point outward from the H4 helix and the C-terminus. These basic residues (Arg 34, Arg 41, Arg 46, Arg 47, Lys 54, Lys 74, Arg 91) define positively charged patches on one face of the protein (Fig. 5B) that could be potential interaction sites between the protein and the negatively charged head groups of the membrane.

Lipid binding

Lysolecithins were chosen as model phospholipids because they exhibit in aqueous solution a simple and rapid equilibrium between dispersed monomeric molecules and micellar aggregates, compatible with NMR techniques. Furthermore, we have previously shown that a lipid–protein complex can be observed easily with monoacyl-lecithins, but not with diacyl-phospholipids. Lysolecithin binding to ns-LTPs induces an increase of the helix content and allows protein crystallization (Rickers et al., 1984; Desormeaux et al., 1992).

Lipid binding by ns-LTPs was first investigated in aqueous solution by fluorescence spectroscopy using as substrates lyso-

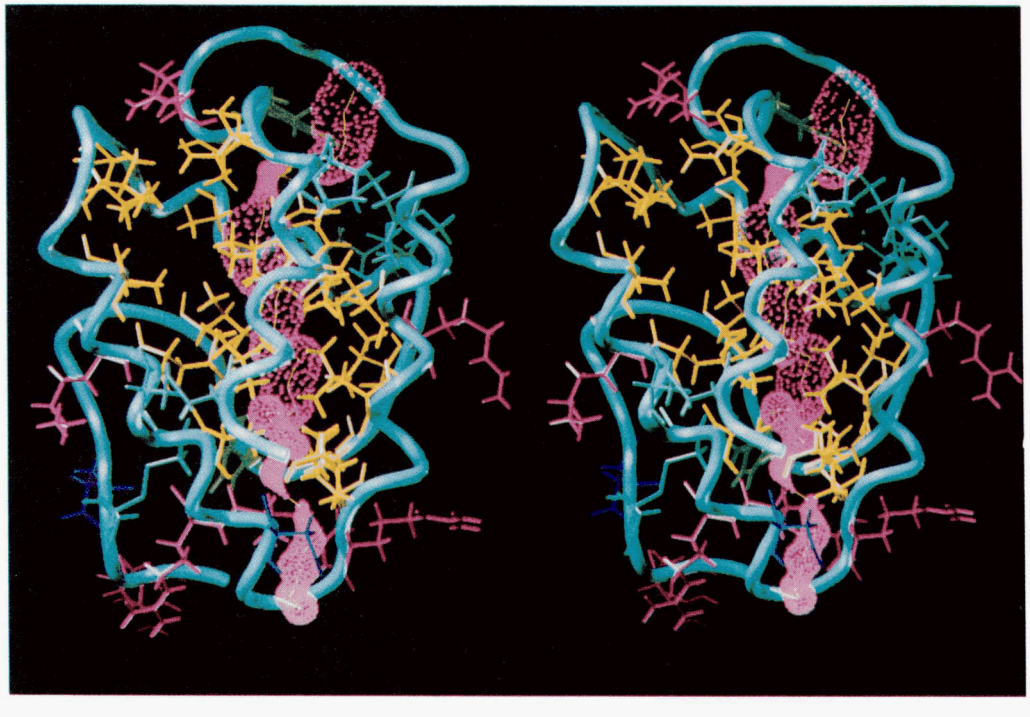

Fig. 4. Stereo view of the pore through the maize ns-LTP. The backbone is represented as a tube colored in cyan, hydrophobic residues lining the cavity are colored in yellow, basic residues in pink, acidic residues in blue, Tyr 17 and Tyr 81 in green, cysteines residues in blue-green, and pink circles show the surface of the cavity, calculated with the PORE program (Smart et al., 1993).

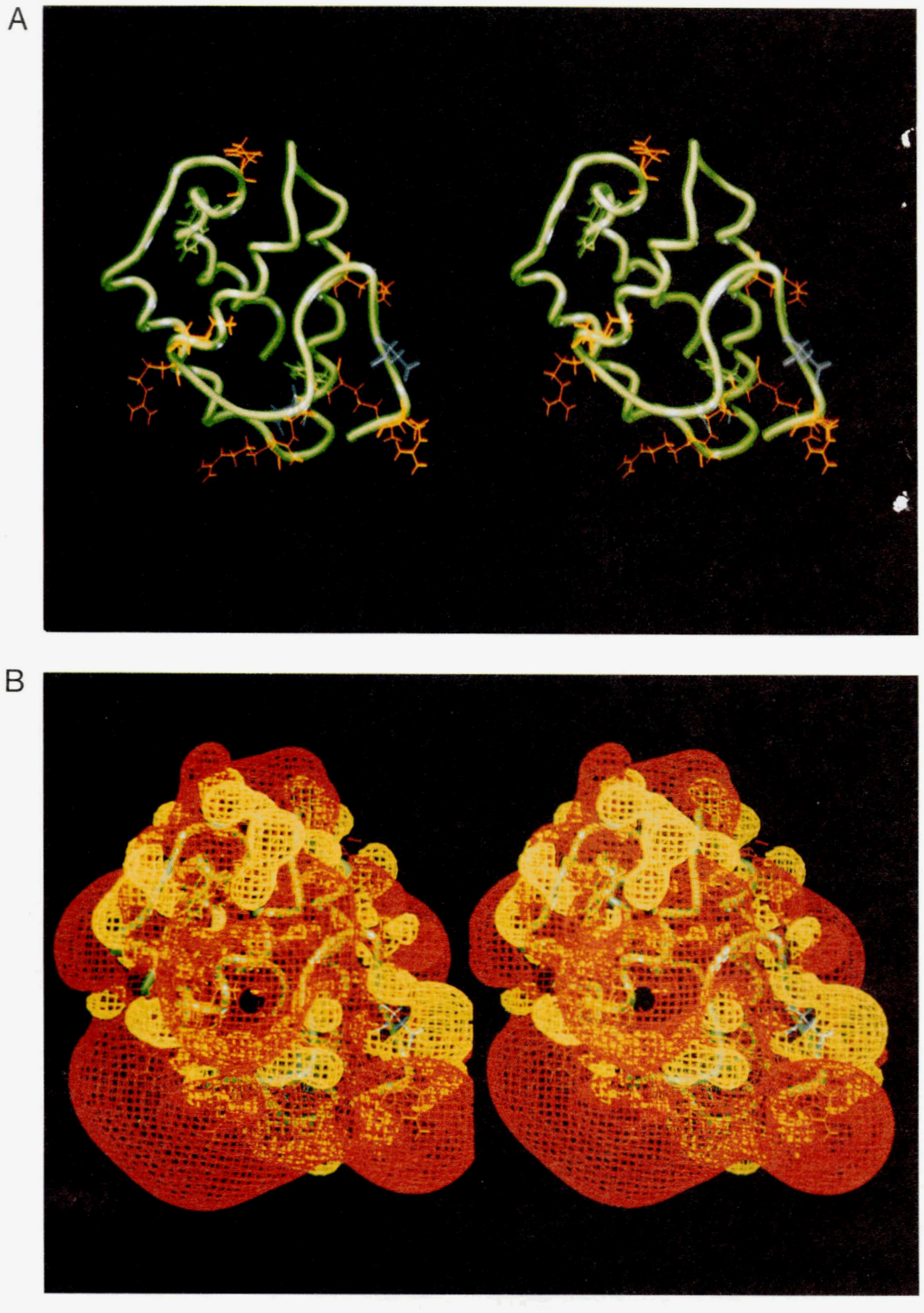

Fig. 5. Charged amino acid distribution and electrostatic potential map of the maize ns-LTP. **A:** Tube representation of the Cα trace of one NMR structure of maize ns-LTP. Side chains of charged residues are represented, colored in orange for basic residues, in blue for acidic residues. **B:** MOLCAD electrostatic potential map representation. Standard Pullman partial charges were included in the calculation. Positive (red) and neutral (yellow) contours are evaluated at +10 kcal mol^{-1} and 0 kcal mol^{-1}, respectively.

C_{16} ($n = 14$) and lyso-C_{12} ($n = 10$), respectively: CH_3-$(CH_2)_n$-CO_2-CH_2-$CH(OH)$-CH_2-PO_4^--$(CH_2)_2$-$N^+(CH_3)_3$.

For the maize protein, lipid binding induces an increase in fluorescence intensity, as illustrated in Figure 6, which is only due to Tyr 17 and Tyr 81 residues present in the H1 helix and C-terminus, respectively. The specific contribution of each fluorophore cannot be determined in such experiments. At lyso-C_{16} saturation, the relative increase of the global fluorescence

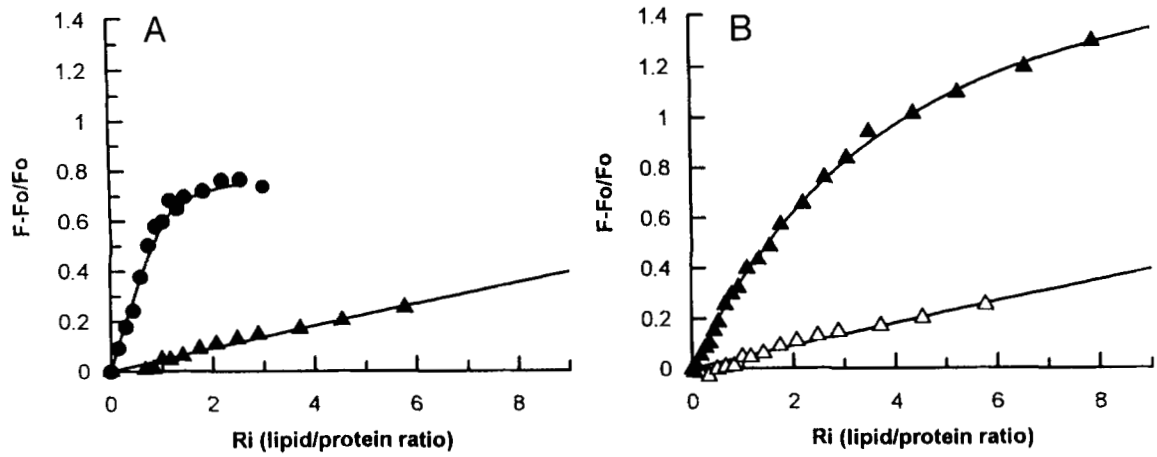

Fig. 6. Relative increase of ns-LTP fluorescence intensity at 310 nm on lysolecithin binding. **A:** Maize ns-LTP and lyso-C_{16} (●) and lyso-C_{12} (▲). **B:** Wheat ns-LTP (▲) and maize ns-LTP (△) with lyso-C_{12}.

intensity is about 80% for the maize ns-LTP (Fig. 6A) and about 120% for the wheat protein (results not shown). For the maize protein with the lyso-C_{12}, this relative increase is much lower. At a lipid/protein ratio (Ri) equal to 6, the relative increase of the global fluorescence is only 20% and does not reach a plateau. On the other hand, the relative increase of fluorescence intensity saturates around 120% for the wheat ns-LTP (Fig. 6B). Curve fitting gives the following values for the dissociation constants, K_d: 10.1 ± 1.2 and 1.9 ± 0.6 × 10^{-6} M for the interaction of lyso-C_{16} and 150 ± 8 × 10^{-6} M and >1 × 10^{-3} M for the interaction of lyso-C_{12} with wheat and maize ns-LTPs, respectively. The K_d values obtained with lyso-C_{16} are in the same order of magnitude as was found (4 × 10^{-6} M) for the binding of long-chain fatty acids by an oat ns-LTP (Rickers et al., 1984). The difference in the affinity between maize and wheat ns-LTPs for long-chain lysolecithins is significant, but not considerable, whereas the maize protein catalyzes more efficiently phosphatidylcholine transfer between membranes (Petit et al., 1994). This emphasizes the fact that interactions between ns-LTPs and lipid bilayer interfaces are other essential parameters for the transfer of lipids between membranes. The maize protein exhibits a higher affinity with long-chain lysolecithins than does the wheat protein, but a lower affinity with short-chain lipids. This apparent contradiction might be explained by the fact that, under our experimental conditions, lyso-C_{12} is below its critical micellar concentration (CMC = 0.43 × 10^{-3} M), whereas lyso-C_{16} is above (4 × 10^{-6} M). These results suggest that, in the case of the maize protein, lipid binding can occur mainly if lipid aggregates (micelles) are present. Such an interfacial activation is not necessary for the wheat protein, which can bind monomeric lipids.

Lysolecithins binding by ns-LTPs was also investigated by NMR. The results (P. Sodano, unpubl. results) can be summarized as follows. Rather similar behaviors are observed for wheat and maize ns-LTPs in the presence of lyso-C_{16} and lyso-C_{12} (Petit, 1994). Line broadening and changes in ^{1}H chemical shifts, as well as in the scalar and dipolar connectivities, were observed when the proteins were titrated with the lipids. Briefly, for the wheat protein interacting with lyso-C_{16}, a slow exchange between free and bound forms is observed. This is evidenced by the simultaneous observation of NOESY cross peaks arising from both forms in the spectrum for Ri < 1. Based on chemical-shift variations of C_βH protons of Tyr 81, the exchange rate upper limit was estimated at 370 s^{-1}, indicating a slow exchange on the NMR time scale. With lyso-C_{12}, the exchange rate was higher, with a continuous variation of the chemical shifts pointing to a progressive transition between free and bound forms.

Similar results are obtained for the maize protein. A 1/1 lipid-protein complex is formed with palmitoyl and a fast equilibrium is also observed with the lauroyl derivative. In one-dimensional ^{1}H NMR spectra of the complexes, the strong resonance of the CH_2 groups of the lipid aliphatic chain is either totally split and/or broadened and thus undetectable, whereas the resonance of the choline $N^+(CH_3)_3$ group remains narrow (Petit, 1994), which proves that this part of the lipid remains highly mobile. Because overlapping problems precluded unambiguous assignments of NOEs between the lipid and the protein in the complex, we used CαH chemical-shift differences between the free and the bound protein states as probes for locating the lipid-binding site. As seen in Figure 7A, the most dramatic changes for both complexes occur in the second half of the protein sequence whereby the H3, H4 helices and the C-terminus are mainly concerned. Because most hydrophobic residues present in the internal cavity (see above) are affected by lipid complexation, one can assume that this cavity is the binding site of the aliphatic chain of the lipid.

Lipid protein complex

Because the cavity is extended through the entire molecule, opposite orientations of the lipid inside the protein cavity can be considered. Our choice was based on the following arguments. First, a favorable site for the fixation of the polar head exists around the L2 loop in the presence of three positively charged residues (Arg 41, Arg 46, and Arg 47) and one negatively charged residue (Asp 45). This Asp-Arg sequence is especially well conserved in ns-LTPs (Desormeaux et al., 1992). Secondly, as seen in Figure 7B, the Leu 63 C_αH chemical shift is more

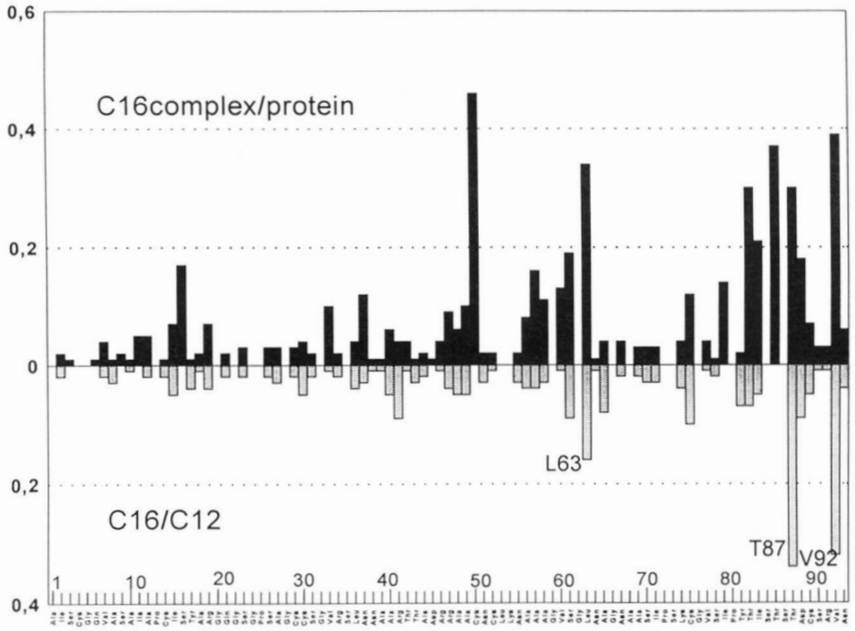

Fig. 7. Hα chemical shifts. The absolute values of the Hα chemical-shift differences in ppm are plotted against residue numbers. Lyso-C_{16} complex and free protein (black bars in the upper part of the histogram). Lyso-C_{16} and lyso-C_{12} complexes (grey bars in the lower part).

perturbed by the long alkyl chain of lyso-C_{16} than by that of lyso-C_{12}.

The hypotheses used to build a model for a complex with lyso-C_{16} in accordance with the NMR data were the embedding of the lipid alkyl chain in the protein cavity with its methyl end close to Leu 63, the anchoring of the phosphate group to the L2 loop charged residues, and the external positioning of the choline head group. The resulting energy-minimized model is shown in Figure 8 and Kinemage 3, where basic residues Arg 41, Arg 46, and Arg 47 interact with the phosphate and Asp 45 is directed toward the positively charged choline moiety. No major differences are observed between free and bound protein structures, except for a slight swelling of the global structure to accommodate the lipid (see Fig. 9 for a superposition of the C_α traces). The average RMSD is 1.1 Å, but the N-terminal part of the protein is less perturbed than the C-terminal part (the RMSD is 0.77 Å for residues 1–60 and 1.29 Å for residues 61–93). Figure 9 shows the Tyr 81 residue is also perturbed by the lipid binding as its aromatic ring, which obstructs the cavity in the free protein, undergoes a 90° rotation, making it nearly parallel to the cavity wall ($\Delta\chi_1 = -17°$, $\Delta\chi_2 = -30°$). In the model, a hydrogen bond between the lipid carbonyl and the proton of the hydroxyl group of Tyr 81 stabilizes the position of the side chain. Such a change in the environment of the tyrosine side chain could explain the 0.31-ppm shift of the ring proton resonances observed in the NMR spectra, as a consequence of the rotation of its aromatic ring. This change of conformation is further supported by the chemical-shift difference observed for $C_\beta H$ protons of Tyr 81 ($\Delta\delta = 0.1$ ppm in the free protein, $\Delta\delta = 0.8$ ppm in the complex). Large chemical-shift changes are also observed for Thr 85 and Val 92, which are in the vicinity of the tyrosine residue. Conversely, Tyr 17 at the end of the H1 helix is solvent exposed and not affected by lipid complexation (Fig. 7). It could then be suggested that fluorescence changes (Subirade et al., 1995) on lysolecithin binding are mainly due to Tyr 81.

Discussion

Comparison of solution and crystal structures

While our work on the NMR determination of the maize ns-LTP three-dimensional structure in solution was terminating, its X-ray structure at 1.9 Å resolution was published (Shin et al., 1995). Because the X-ray coordinates are not yet available, we cannot compare the solution and crystal structures of this protein at the atomic level. A visual inspection shows that both global folds are very similar, except in the C-terminal region, which contains one turn of 3_{10}-helix (89–91) in the crystal and a turn stabilized by the side-chain–backbone hydrogen bond in the solution structure. The slightly different lengths of the H1 and H2 helices are 4–18 and 27–39 in the crystal and 5–19 and 26–39 in solution, respectively. Such differences could reflect environmental effects, but could also originate from the criteria used to define the helical residues, DSSP in our calculations (Kabsch & Sander, 1983).

There is a good correlation between the variations of the backbone average RMSD of the NMR-derived structures and the backbone *B*-factors of the X-ray structure (Shin et al., 1995), which indicates both static and dynamic disorder in the crystal. Clearly, these disorders are higher in the three loops and the C-terminal fragment than in the four helices. The end of this last fragment is less structured in solution than in the crystal form (no 3_{10}-helix is observed). Two additional residues (Val 7 and Ala 10) are found to be involved in the internal hydrophobic cavity in the solution structure. The volume of this cavity, estimated at 270 $Å^3$ in the models of the solution structure, is the same or-

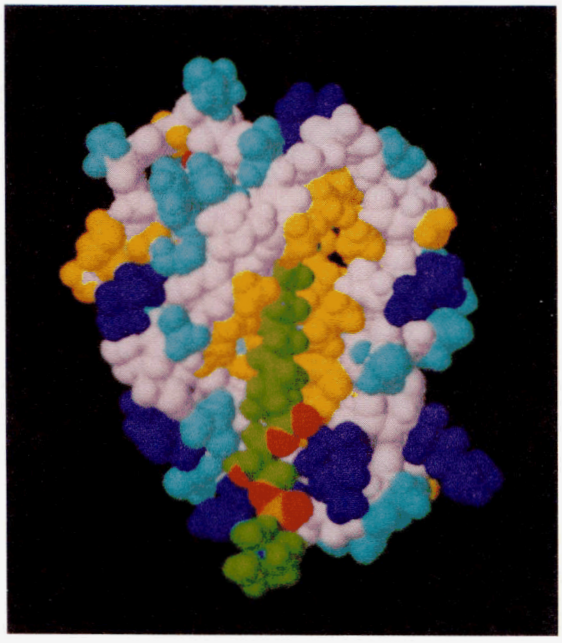

Fig. 8. Space-filling model of the lyso-C_{16}–maize ns-LTP complex. The residues Gly 76–Asn 93 are not displayed in order to show the embedding site of the lipid. Colors are coded as follows: lipid in green with phosphate and carbonyl groups colored by atom type, protein backbone in white, hydrophobic side-chains in yellow, basic residues in blue.

der of magnitude (300 $Å^3$) as in the crystal. No ordered specifically bound water molecules were detected in the hydrophobic cavity by X-ray diffraction.

There are no major differences between the backbone folds of the free and the palmitate-complexed ns-LTP crystal structures (Shin et al., 1995). Interestingly, the *B*-factors of the complexed form are reduced in the second part of the protein sequence, exactly where the $C_\alpha H$ chemical shifts are more perturbed by complexation of the ns-LTP with lyso-C_{16}. Our model for the complex is fully consistent with the crystal data. In both structures, the aliphatic chain of the palmitate and lyso-C_{16} are extended inside the internal cavity and their polar heads are orientated toward the L2 loop. Due to the size and structure of its polar head, lyso-C_{16} is probably not located in exactly the same position as the palmitate molecule. A perturbation is detected in the NMR spectra of the C_{16} complex (Fig. 7), around the L3 loop (Leu 63), which could be attributed to the presence of the methyl end of the aliphatic chain. This chain is slightly kinked around the C_2-C_4 and C_{14}-C_{16} bonds; this kink results from a local narrowing of the hydrophobic cavity. Tyr 81 plays a key role in the mechanism of lipid insertion into the hydrophobic cavity (see above) in that its hydroxyl group interacts with the carboxylate or carbonyl group of the lipid in both complexes.

Maize and wheat ns-LTP solution structures

We have previously published the first known three-dimensional structure of a plant ns-LTP issued from an NMR study of the wheat protein in aqueous solution (Gincel et al., 1994), and we have compared the secondary structures of both proteins (Petit et al., 1994). Besides the small structural variations resulting from a better refinement of the structure of this second protein, noticeable differences appear in the H1 and H4 regions. Both H1 helices are kinked around a median Pro residue, but the H1 maize protein fragment is clearly longer than the other (Fig. 10). In the wheat protein, the H4 helix, which exhibits rather scattered (ϕ,ψ) angles and is closed to a 3_{10}-helix, is interrupted by two consecutive prolines. The three residues that follow in the sequence remain in helical conformation. In the maize protein, H4 is a well-defined α-helix that is only slightly distorted by a

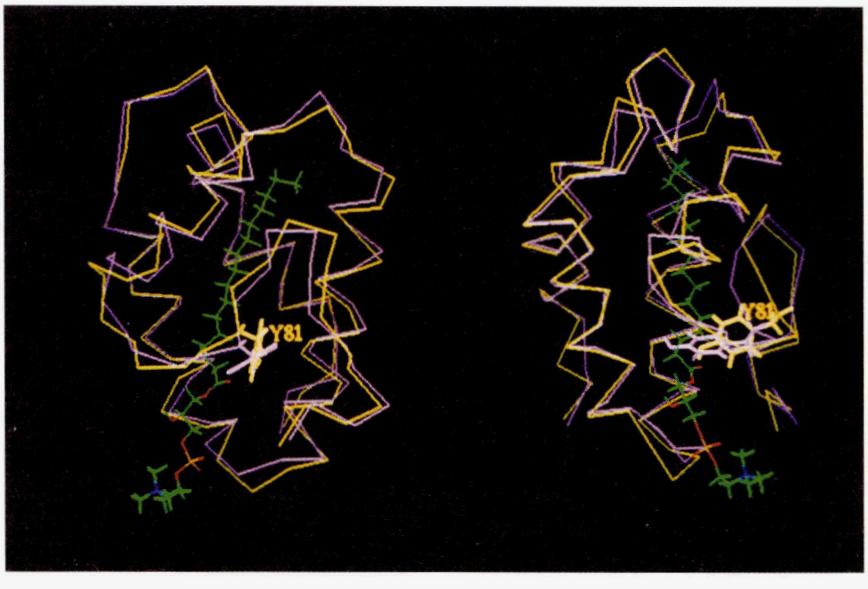

Fig. 9. Complex and free protein backbone comparison. The protein Cα trace is represented in an orthographic view. Color coding is the same as in Figure 10. The swing of the crucial Tyr 81 aromatic ring, which is displayed in magenta for the free protein and in yellow in the complex, is highlighted.

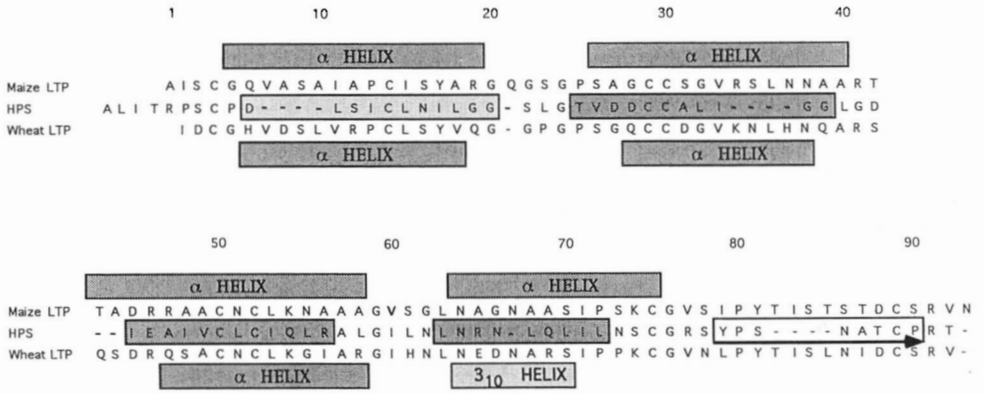

Fig. 10. Sequence alignment of HPS, wheat, and maize ns-LPT. Secondary structure elements are indicated. Arrow corresponds to a β-strand.

unique Pro residue. Some differences also exist at the C-terminus, in which a short γ-turn is found at residue 83 in the wheat protein, whereas the corresponding turn in the maize ns-LTP is looser and stabilized by hydrogen bonds involving side chains. Our present results indicate that the L2, H3, H4, and C-terminus are probably involved in the lipid complexation mechanism. However, it seems premature to draw any conclusions about the relationships between the three-dimensional structures of wheat and maize ns-LTPs and their different transfer activities. The transfer activity is a global mechanism involving interactions between ns-LTPs and membranes and the formation of lipid–protein complexes. The next step in our investigation will be to establish the structure of a wheat ns-LTP–lyso-C_{16} complex and to compare this model to the maize ns-LTP complex described here.

ns-LTPs and HPS structures

HPS is a small globular protein whose structure was resolved at a resolution of 1.8 Å by X-ray diffraction (Baud et al., 1993). NMR studies of the protein were begun in our laboratory and a similar secondary pattern was found in solution (Sodano & Ptak, 1995). The protein sequence contains 80 amino acids and eight cysteines forming four disulfide bridges; 40% sequence similarities were found with other ns-LTPs. The authors described the protein structure as a four-helix right-handed bundle with a C-terminus packed against the fourth helix in a β-strand conformation. The main feature of this protein is the very high number of hydrophobic residues, which are partly exposed to the solvent. As a consequence, its solubility in aqueous solution is very poor at neutral pH and, therefore, its biological function is still unknown. Similarities exist between the structures of wheat and maize proteins on the one hand and that of the soybean protein on the other. The three proteins adopt similar architectures, as emphasized by the interhelical angle values listed in Table 3. Furthermore, in HPS, most of the hydrophobic residues were found to be involved in the formation of a hydrophobic core. Close examination of the structure shows the existence of a hydrophobic tunnel, not described previously. The cavity runs parallel to the H3 helix through the whole molecule, starting at the L2 loop and ending at the L1. The cavity volume is roughly the same order as those found for wheat and maize ns-LTPs.

On the contrary, it is worth noting some striking differences. First, the net charge of the HPS is null at neutral pH. Secondly, no polar residue is pointing inside the cavity, which could potentially form a hydrogen bond with a carbonyl group of a lipid (Tyr 71 juts out into the solvent). Furthermore, only one negatively charged residue is present in the L2 loop, whereas in ns-LTPs, a cluster of positive and negative residues in this loop stabilizes the lipid–protein complex. From these observations, it is premature to conclude that the HPS is a lipid carrier despite the similarities to the two ns-LTPs. The presence of the channel seems to be inherent in the spatial arrangement of the four helices, maintained by four disulfide bridges, which defines a novel architecture of α-proteins.

Lipid transfer activity

The present results demonstrate that, just as the wheat ns-LTP, the maize ns-LTP is able to complex a lysolecithin in aqueous solution. However, unlike the wheat protein, an interfacial activation is apparently necessary to bind the lipids. Lysolecithins exhibit a lower affinity for the maize ns-LTP below their critical micellar concentration. Interfacial activation is also encountered in the lipid hydrolysis by phospholipases (Scott & Sigler, 1994), and is in agreement with previous fluorescence results indicating that the maize protein (and not the wheat) induces important changes in the structure and dynamics of the liposome

Table 3. *Mean interhelical angles (in degrees) calculated according to Harris et al. (1994)*

	Maize ns-LTP	Wheat ns-LTP	HPS
(2,1)	−146	−143	−137
(3,1)	− 31	−22	−65
(3,2)	−141	−143	127
(4,1)	124	132	100
(4,2)	−78	−72	−101
(4,3)	140	145	126

lipids (Subirade et al., 1993). Therefore, compared to the wheat ns-LTP, the higher interfacial activity of the maize protein could be responsible for its higher transfer activity.

Lipid transfer obviously implies adsorption of the ns-LTP on the bilayer interfaces before the binding occurrence. We have previously shown that lipid transfer activity is improved by increasing the anionic phospholipid ratio in liposomes (Petit et al., 1994). This improvement could be related to the charged residue distribution and the subsequent electrostatic potential repartition (Fig. 5). Indeed, the maize ns-LTP has a positively charged side, involving the H3 helix and the C-terminus, which could be a potential interaction site with negatively charged membrane interfaces. Clearly, the remaining problem is to determine the mode of binding of diacyl-phospholipids to ns-LTPs. As demonstrated by solution and crystal studies, the tunnel-like cavity can accommodate one aliphatic chain without major changes in the protein structure.

The existence of a stable lysolecithin–protein complex in aqueous solution is compatible with a model in which the ns-LTP acts as a carrier capable of extracting one lipid molecule from a membrane and transferring it to another. Until now, it was impossible to isolate a stable complex involving diacyl phospholipids and to establish the mode of binding of such a molecule to the ns-LTP. Recent monolayer experiments (Subirade et al., 1995) give some new information on the interaction between the wheat ns-LTP and diacylphospholipids. A model is proposed involving a collisional complex-shuttle mechanism. In this model, only one acyl chain of the lipid is inserted into the protein hydrophobic tunnel and the transfer implies a close contact between the donor and acceptor membranes to avoid transfer of the second acyl chain in the aqueous solvent. New investigations are currently undertaken in order to establish more precisely the binding mode of diacylphospholipids by ns-LTPs.

Materials and methods

Fluorescence spectroscopy

Binding of lysophosphatidylcholine species was probed by intrinsic fluorescence spectroscopy of tyrosine residues of wheat and maize LTPs. Experiments were conducted at 25 °C with a SLM 4800 spectrofluorimeter (Aminco, USA). The excitation wavelength was at 275 nm and emission spectra were recorded from 300 to 400 nm with 4-nm bandwidths and were corrected for the buffer contribution. Inner filter effect was negligible by maintaining sample absorbency below 0.1 absorbency units. Small amounts of concentrated dodecanoyl- and hexadecanoyllysophosphatidylcholine solutions in water (1–5 mg/mL) were added stepwise to a cuvette containing 1 mL of a LTP solution (0.25 mg/mL) in 20 mM Tris-HCl, pH 7.8, in order to limit volume changes (maximum increase 5% at the end of a binding assay). For each lipid–protein ratio, the fluorescence maximum intensity at 310 nm was used for constructing lipid titration curves. This maximum intensity was determined by averaging the intensity values obtained at 309, 310, and 311 nm. Curve fitting was carried out by considering one binding site from NMR lipid titration experiments. The quality of fitting was assessed by a reduced χ_2 test. Free ligand (L) was determined by $L = L_0 - \alpha P_0$, where L_0 and P_0 are the total lipid and protein concentrations in mM; α is the fraction of the occupied site determined as $(F - F_0/F_{max} - F_0)$, where F_0 is the fluorescence intensity of the protein solution, F_{max} the maximum intensity obtained at lipid saturation, and F the intensity obtained at each lipid–protein ratio.

NMR-derived geometric constraints

The samples of wheat and maize ns-LTPS were purified as described previously (Desormeaux et al., 1992). Experimental conditions of the ^{1}H NMR study of the maize ns-LTP have been described elsewhere (Petit et al., 1994). Upper-bound distance restraints were derived from two sets of NOESY spectra recorded on a Bruker AMX-500 spectrometer operating at a frequency of 500 MHz for proton nucleus on a 10-mM sample of maize ns-LTP in 90% H_2O/10% D_2O solution buffered at pH 5.5 by deuterated-acetate (100 mM). For spectra recorded in D_2O, a 4-mM sample was used (40 mM of acetate buffer) under the same experimental conditions. For all spectra, the spectral width was 5,050 Hz and the temperature was set to 308 K. The quantitative distances were derived from NOESY spectra recorded with mixing times of 60 and 120 ms. For each NOESY experiment, 800 t_1 values were recorded with 4,096 data points along the t_2 dimension. Prior to Fourier transformation, the time domain data were multiplied by phase-shifted sine-bell functions and zero filled to 8,192 points in t_2 and 2,048 in t_1. Spin-spin coupling constants $^3J_{\alpha NH}$ were measured on a high-resolution DQF-COSY spectrum recorded with 800 t_1 values and 8,192 points along t_2 and zero filled to 2,048 points in t_1 and 16,384 points along t_2. $^3J_{\alpha\beta}$ coupling constants were derived from a ECOSY spectrum recorded with 800 points along t_1 and 8,192 points along t_2 and zero filled to 2,048 points along t_1 and 16,384 points along t_2 prior to Fourier transform.

The studies on lipid–protein complexes were conducted on 2–3-mM samples of protein. The solutions were buffered at pH 5.5 by deuterated acetate and spectra were recorded at 308 K. Increasing amounts of lyso-phospholipids were added to the protein solution from 0 to 3 equivalents by steps of 0.5 equivalent. At each step, a one-dimensional and a NOESY spectrum were recorded. Chemical shifts of the protein protons in the complexes were measured on NOESY spectra recorded on samples containing three equivalents of lyso-phospholipids for both complexes with C_{12} and C_{16} lipids.

Structure determination

The three-dimensional structure of the maize ns-LTP in solution has been determined by a hybrid method based on distance geometry and simulated annealing procedures. The assignment of the NOESY cross peaks was supported by repeated rounds of structure calculations with DIANA and ASNO software. The cross peak volumes, obtained from the NOESY experiments recorded in H_2O, were corrected to restore the initial signal before the jump and return sequence. After internal calibration, the interproton NOEs were classified into 10 qualitative bands provided by the CALIBA program. Before application of the appropriate pseudo-atom correction (Wüthrich et al., 1983), the values for the upper distance limits were restricted to the 2.4–5.0-Å range for NOEs recorded at 60 ms. The upper distance limit was set at 6.0 Å for NOEs observed at 120 ms. Restraints for backbone and side-chain torsional angles were derived from the 120 measured coupling constants ($^3J_{NH\alpha}$ and $^3J_{\alpha\beta}$) and intraresidual and sequential distances by using the systematic grid-

search method included in the HABAS program. Twenty prochiral groups were stereospecifically assigned using HABAS and GLOMSA. In addition, we were able to assign stereospecifically methyl protons of four out of five valine residues. The final structure calculations, performed with DIANA using the REDAC strategy, were based on 1,091 NOE-derived distance restraints (Fig. 3A) including 162 intra residue, 283 sequential, 333 medium-range ($1 < |i-j| \leq 4$), and 313 long-range connectivities, and 197 dihedral restraints (79 ϕ, 80 ψ, 38 χ_1). We added 20 constraints defining the four disulfide bridges, and 52 other constraints taking into account 26 hydrogen bonds related to the slow exchange rates in D_2O of the amide protons in the regular secondary structure. A set of 26 structures with low DIANA target function (0.6–2 Å^2) was further refined by using standard XPLOR (Brünger, 1992) simulated-annealing protocols and energy minimization with the CHARMM (Brooks et al., 1983) force field potential implemented in XPLOR 3.1.

The disulfide pairing of the eight cysteine residues of the maize LTP was not characterized chemically, but was deduced in the course of the structure determination. This was achieved by an analysis of the S-S distances in a set of 50 DIANA structures calculated without the specific inclusion of disulfide bonding information.

The secondary structure of each member of the ensemble was determined using the method of Kabsch and Sander (1983). Out of 26 XPLOR energy-minimized structures, 15 were selected using the following criteria. The final structures exhibit no extra constraint violations compared to the DIANA structures (starting point of XPLOR calculations and present at least 70% of their (ϕ,ψ) torsional angles in the core region of the Ramachandran maps).

The modeling study of the complexes with α-lysopalmitoylphosphatidylcholine (lyso-C_{16}) was carried out with the SYBYL software (TRIPOS, St. Louis, Missouri). The starting structures were built up by visual docking of the lipid molecule into the maize ns-LTP according to the previous results of the NMR study. These initial structures were then minimized using the TRIPOS force field (Clark et al., 1989), with a 10-Å cut-off distance, Pullman atomic charges, and a distance-dependent dielectric function $\epsilon = 3r$ in order to simulate the solvent effect. The first minimization involved the lipid atoms and the residues of the hydrophobic pocket and in a second step, all the side-chain atoms were included in the minimization process. The final minimization included the whole set of atoms of the complex. Coordinates of the solution structure of maize ns-LTP have been deposited in the Brookhaven Protein Data Bank.

Acknowledgments

We thank Anita Caille for the analysis of two-dimensional NMR data, and Jean-Pierre Compoint and Geneviève Compoint in the purification of lipid transfer proteins and the lipid binding studies by fluorescence spectroscopy. This work was supported by the Centre National de la Recherche Scientifique (C.N.R.S.), the Institut National de la Recherche Agronomique (I.N.R.A.), the Région Centre, the Région Pays de Loire, and the Université d'Orléans. It forms part of Jérôme Gomar's thesis, supported by a BDI grant. We also thank the C.I.T.U. for a grant of time on their computers.

References

Aguirre PJ, Smith AG. 1993. Molecular characterization of a gene encoding a cysteine-rich protein preferentially expressed in anthers of *Lycopersicon esculentum*. *Plant Mol Biol 23*:477–487.

Baud F, Pebay-Peroula E, Cohen-Addad C, Odani S, Lehmann MS. 1993. Crystal structure of hydrophobic protein from soybean; a member of a new cysteine-rich family. *J Mol Biol 231*:877–887.

Bernhard WR, Thoma S, Botella J, Somerville CR. 1991. Isolation of a cDNA clone for spinach lipid transfer protein and evidence that the protein is synthesized by the secretory pathway. *Plant Physiol 95*:164–170.

Bowles DJ. 1990. Defense-related proteins in higher plants. *Annu Rev Biochem 59*:893–907.

Brooks BR, Bruccoleri RE, Olafson BD, States DJ, Swaminathan S, Karplus M. 1983. CHARMM: A program for macromolecular energy minimization and dynamics calculations. *J Comput Chem 4*:187–217.

Brünger AT. 1992. *The X-PLOR software manual, version 3.1*. New Haven, Connecticut: Yale University.

Clark M, Cramer RD, van Opdenbosch N. 1989. Validation of the general purpose Tripos 5.2 force field. *J Comput Chem 10*:982–1012.

Coutos-Thevenot P, Jouenne T, Maes O, Guerbette F, Grosbois M, Le Caer P, Boulay M, Deloire A, Kader JC, Guern J. 1993. Four 9-kDa proteins excreted by somatic embryos of grapevine are isoforms of lipid-transfer proteins. *Eur J Biochem 217*:885–889.

Crain RC, Zilversmitt DB. 1980. Two nonspecific phospholipid exchange proteins from beef liver. 1. Purification and characterization. *Biochemistry 19*:1433–1439.

Desormeaux A, Blochet JE, Pezolet M, Marion D. 1992. Amino acid sequence of a non-specific wheat phospholipid transfer protein and its conformation as revealed by infrared and Raman spectroscopy. Role of disulfide bridges and phospholipids in the stabilization of the α-helix structure. *Biochim Biophys Acta 1121*:137–152.

Fleming AJ, Mandel T, Hofman S, Sterk P, de Vries SC, Kuhlemeier C. 1992. Expression pattern of a tobacco lipid transfer protein gene within the shoot apex. *Plant J 2*:855–862.

Foster GD, Robinson SW, Blundell RP, Roberts MR, Hodge R, Draper J, Scott RJ. 1992. A *Brassica napus* mRNA encoding a protein homologous to phospholipid transfer proteins, is expressed specifically in the tapetum and developing microspores. *Plant Sci 84*:187–192.

Gausing K. 1994. Lipid transfer protein genes specifically expressed in barley leaves and coleoptiles. *Planta 192*:574–580.

Geldwerth D, de Kermel A, Zachowski A, Guerbette F, Kader JC, Henry JP, Devaux PF. 1991. Use of spin-labeled and fluorescent lipids to study the activity of the phospholipid transfer protein from maize seedlings. *Biochim Biophys Acta 1082*:255–264.

Gincel E, Simorre JP, Caille A, Marion D, Ptak M, Vovelle F. 1994. Three-dimensional structure in solution of a wheat lipid-transfer protein from multidimensional ^{1}H-NMR data. *Eur J Biochem 226*:413–422.

Güntert P, Braun W, Wüthrich K. 1991. Efficient computation of three-dimensional protein structures in solution from nuclear magnetic resonance data using the program DIANA and the supporting programs CALIBA, HABAS, and GLOMSA. *J Mol Biol 217*:517–530.

Güntert P, Qian YQ, Otting G, Müller M, Gehring W, Wüthrich K. 1993. The program ASNO for computer-supported collection of NOE upper distance constraints as input for protein structure determination. *J Biomol NMR 3*:601–606.

Harris NL, Presnell SR, Cohen FE. 1994. Four helix bundle diversity in globular proteins. *J Mol Biol 236*:1356–1368.

Heiden W, Goetze T, Brickman J. 1993. Fast generation of molecular surfaces from 3D data fields with an enhanced marching cube algorithm. *J Comp Chem 14*:246–251.

Kabsch W, Sander C. 1983. Dictionary of protein secondary structure: Pattern recognition of hydrogen-bonded and geometrical features. *Biopolymers 22*:2577–2637.

Kader JC. 1990. Intracellular transfer of phospholipids, galactolipids and fatty acid in plant cells. In: Hilderson HJ, ed. *Subcellular biochemistry*. New York: Plenum Publishing Corporation. pp 69–111.

Laskowski RA, MacArthur MW, Moss DS, Thornton JM. 1993. PROCHECK: A program to check the stereochemical quality of protein structures. *J Appl Crystallogr 26*:283–291.

MacArthur MW, Thornton JM. 1991. Influence of proline residues on protein conformation. *J Mol Biol 218*:397–412.

Meijer EA, de Vries SC, Sterk P, Gadella DW, Wirtz K, Hendriks T. 1993. Characterization of the non-specific lipid transfer protein EP2 from carrot (*Daucus carota* L.) *Mol Cell Biochem 123*:159–166.

Miquel M, Block M, Joyard J, Dorne AJ, Dubacq JP, Kader JC, Douce R. 1987. Protein-mediated transfer of phosphatydidycholine from liposomes to spinach chloroplast envelope membranes. *Biochim Biophys Acta 937*:219–228.

Molina A, Segura A, Garcia-Olmedo F. 1993. Lipid transfer proteins (nsLTPs) from barley and maize leaves are potent inhibitors of bacterial and fungal pathogens. *FEBS Lett 316*:119–122.

Ostergaard J, Vergnolle C, Schoentgen F, Kader JC. 1993. Acyl-binding/lipid

transfer protein from rape seedlings, a novel category of proteins interacting with lipids. *Biochim Biophys Acta 1170*:109–117.

Pelese-Siebenbourg F, Caelles C, Kader JC, Delseny M, Puigdomenech P. 1994. A pair of genes coding for lipid-transfer proteins in *Sorghum vulgare*. *Gene 148*:305–308.

Petit MC. 1994. Etude par RMN 2D de la structure tridimensionnelle en solution aqueuse, de proteines de transfert de lipides et de leurs interactions avec des lipides [thesis]. Paris VI: University Pierre et Marie Curie.

Petit MC, Sodano P, Marion D, Ptak M. 1994. Two- and three-dimensional 1H NMR studies of maize lipid-transfer protein. Sequence specific assignment and secondary structure. *Eur J Biochem 222*:1047–1054.

Pyee J, Yu H, Kolattukudy PE. 1994. Identification of a lipid transfer protein as the major protein in the surface wax of broccoli leaves. *Arch Biochem Biophys 331*:460–468.

Record E, Lesage L, Marion D, Cahagnier B, Richard-Molard D, Asther M. 1993. Proteine de champignons filamenteux capable de realiser la fixation et le transport des lipides, leurs procedes d'obtention et leurs applications. *Fr Pat Appl* 9301518.

Rickers I, Tober I, Spener F. 1984. Purification and binding characteristics of a basic fatty acid binding protein from *Avena sativa* seedlings. *Biochim Biophys Acta 794*:313–319.

Rueckert DG, Schmidt K. 1990. Lipid transfer proteins. *Chem Phys Lipids 56*:1–20.

Scott DL, Sigler PB. 1994. Structure and catalytic mechanism of secretory phospholipase A2. *Adv Protein Chem 45*:53–87.

Shin DH, Lee JY, Hwang KY, Kim KK, Suh SW. 1995. High-resolution crystal structure of the non-specific lipid-transfer protein from maize seedlings. *Structure 3*:189–199.

Skriver K, Leah R, Muller-Uri F, Olsen FL, Mundy J. 1992. Structure and expression of the barley lipid transfer gene Ltp1. *Plant Biol 18*:585–589.

Smart OS, Goodfellow JM, Wallace BA. 1993. The pore dimensions of Gramicidin A. *Biophys J 65*:2455–2460.

Sodano P, Ptak M. 1995. Secondary structure in solution of the hydrophobic protein of soybean (HPS) as revealed by ^{1}H NMR. *J Biomol Struct Dynam 12*:1009–1022.

Sossountzov L, Ruiz-Avila L, Vignols F, Jolliot A, Arondel V, Tchang F, Grosbois M, Guerbette F, Miginiac E, Delseny M, Puigdomenech P, Kader JC. 1991. Spatial and temporal expression of a maize lipid transfer protein gene. *The Plant Cell 3*:923–933.

Sterk P, Booij H, Schellekens GA, Van Kammen A, de Vries SC. 1991. Cell specific expression of the carrot EP2 lipid transfer protein gene. *The Plant Cell 3*:907–921.

Subirade M, Marion D, Pezolet M. 1993. Interaction of a non-specific maize phospholipid transfer protein with unilamellar vesicles: An infrared spectroscopy study. *S P I E 2089*:346–347.

Subirade M, Salesse C, Marion D, Pezolet M. 1995. Interaction of a non-specific wheat lipid transfer protein with phospholipid monolayers imaged by fluorescence microscopy and studied by infrared spectroscopy. *Biophys J 69*:974–988.

Takishima K, Watanabe S, Yamada M, Suga T, Mamiya G. 1988. Amino acid sequences of two non-specific lipid transfer proteins from germinated castor bean. *Eur J Biochem 177*:241–249.

Thoma S, Hecht U, Kippers A, Botella J, de Vries S, Somerville C. 1994. Tissue specific expression of a gene encoding a cell wall-localized lipid transfer from *Arabidopsis*. *Plant Physiol 105*:35–45.

Torres-Schuman S, Gogoy JA, Pintor-Toro JA. 1992. A probable lipid transfer gene is included by NaCl in stems of tomato plants. *Plant Mol Biol 18*:749–757.

Tsuboi S, Osafune T, Nishimura M, Yamada M. 1992. Nonspecific lipid transfer protein in castor bean cotyledon cells: Subcellular localization and a possible role in lipid metabolism. *J Biochem 111*:500–508.

Vignols F, Lung G, Pammi S, Tremousaygue D, Grellet F, Kader JC, Puigdomenech P, Delseny M. 1994. Characterization of a rice gene coding for a lipid transfer protein. *Gene 142*:265–270.

Weig A, Komor E. 1992. The lipid transfer protein C of *Ricinus communis*: Isolation of two cDNA sequences which are strongly and exclusively expressed in cotyledons after germination. *Planta 187*:367–371.

Wüthrich K, Billeter M, Braun W. 1983. Pseudo-structures for the 20 common amino acids for use in studies of protein conformation by measurements of intramolecular proton–proton distance constraints with nuclear magnetic resonance. *J Mol Biol 169*:949–961.